

# Applying Computational Stress Inference to Examine Mechanical Forces During Dorsal Closure in *Drosophila* Embryogenesis

Jon Recalde<sup>1</sup>

## Abstract

During the study of developmental biology, understanding the dynamic interplay between genetic signals and mechanical forces is crucial. This research focuses on the exploration of these mechanical forces during the morphogenesis of the *Drosophila* embryo, specifically in the process of dorsal closure. By employing the sophisticated and non-invasive stress inference technique, the study aims to analyze the balance of forces throughout this vital process. Using computational methods, we have effectively utilized an approach to quantitatively measure relative tensions within the biological tissue of amnioserosa cells, under the assumption of mechanical equilibrium. Our findings reveal that amnioserosa cells, often considered uniform, exhibit distinctive behaviors influenced by both their surroundings and their position in the tissue. The study also investigated different genotype conditions, in which Myosin II activity, a protein responsible for generating forces, is perturbed, and analyzed how the mechanical state of the tissue varies. Despite challenges in inferring pressures due to the complex dynamics of cell membranes, this research explores the mechanics underpinning developmental processes, highlighting the potential of computational stress inference as a powerful tool for analyzing tissue dynamics.

**Keywords:** Inferred Stress, Mechanical Equilibrium, Dorsal Closure

## 1. Introduction

Morphogenesis, the biological process responsible for the shapes and patterns of an organism, is a cornerstone of developmental biology. Throughout this complex event, cells change shape, migrate, divide and differentiate to give rise to the intricate three-dimensional structures of tissues and organs. The orchestration of these cellular behaviors is directed by two forms of fundamental information: developmental programs of gene expression and mechanical forces (Collinet and Lecuit, 2021).

Genetic signals define intrinsic biochemical pathways and cellular programming, which are vital for cellular functions like differentiation, proliferation, and environmental response mechanisms. Simultaneously, mechanical forces, which have been recognized as critical determinants of morphogenesis for over a century, modulate static and dynamic cellular structures and behaviors, including cell size, shape, number, position, and gene expression (Heer and Martin, 2017; Roffay et al., 2021). These forces, generated by molecular motors like the actomyosin networks, are propagated within the cellular framework via adhesive complexes (Graner and Riveline, 2017).

The interplay between genetics and mechanics, which can regulate each other by feedback mechanisms, ensures robust tissue development within species and accounts for variations observed across different organisms (Miller and Davidson, 2013; Hannezo and Heisenberg, 2019). Intriguingly, morphogenesis and tissue mechanics can reciprocally influence cell-fate specification, highlighting the need for a deeper understanding of the roles of force and stress in tissue morphogenesis (Gjorevski and Nelson, 2010; Mammoto et al., 2012; Chan et al., 2017).

Efforts to quantify these forces and stresses *in vivo* have

led to the development of various techniques such as inserts, contact manipulation, laser ablation and genetically encoded molecular sensors, among others (Roca-Cusachs et al., 2017). While these methods provide invaluable insights, many of them are somewhat invasive and may only offer mechanical information at a single location and time.

Stress inference method stands out in this context due to its non-invasive nature, ability to provide information across multiple positions and time-points, and its relative cost-effectiveness and speed. Leveraging high-quality image data, stress inference can estimate cell-level tensions and pressures, under suitable circumstances and with appropriate side conditions, revealing mechanical interactions across a tissue based solely on the geometries obtained by image analysis (Taylor, 1976; Cantat et al., 2013; Roffay et al., 2021).

Stemming from the pioneering ideas by Thomson (1917), stress inference gained validation and feasibility through Stein and Gordon (1982)'s soap bubble froth analogy. With the advent of the 21st century and fueled by advances in computational and live imaging techniques, the technique saw notable improvements. Initially designed for two-dimensional studies by Chiou et al. (2012), it provided insights into various developmental processes, such as *Drosophila* pupal dorsal thorax and wing morphogenesis (Ishihara and Sugimura, 2012; Guirao et al., 2015) and germband extension (Noll et al., 2020). Its recent adaptation to three-dimensional analyses, such as in zebrafish gastrulation (Krens et al., 2017), emphasizes the method's versatility and its growing role in developmental biology.

This research aims to harness the power of stress inference to

explore the contribution of mechanical signals during morphogenesis using the process of dorsal closure of the *Drosophila* embryo as a model system. With its potential to provide insights at both cellular and tissue scales, stress inference promises to enhance our understanding of the complex mechanics underpinning developmental processes.

## 2. Dorsal Closure in *Drosophila*

Dorsal closure is a critical process in *Drosophila* embryogenesis, during which the embryonic lateral epidermis migrates to enclose the amnioserosa, a transient extra-embryonic tissue, thereby to form a continuous dorsal epidermis. This process is a well-studied example of tissue morphogenesis and involves co-ordinated cell shape changes and cell movements of two tissues, the amnioserosa and the epidermis (Figure 1). A supra-cellular actomyosin cable that forms at the interface between these two tissues also provides a major contribution to the process (Jacinto et al., 2002; Gorfinkiel et al., 2011; Kiehart et al., 2017).

1. *Amnioserosa*: The amnioserosa is a single-layer epithelial sheet that provides the driving force for dorsal closure through apical constriction. The cells of this transient tissue at the embryo's dorsal side engage in pulsatile contractions, which are primarily driven by the rhythmic assembly and disassembly of the actomyosin networks within these cells. The contractions, in combination with apical constriction of the cells, generate forces that aid in the movement of the lateral epidermis toward the dorsal midline. Additionally, delamination and apoptosis (programmed cell death) of around 10% amnioserosa cells further contribute to the progression of dorsal closure (Solon et al., 2009; Gorfinkiel et al., 2009; Blanchard et al., 2010). From a biomechanical perspective, as stated by Hutson et al. (2003), the amnioserosa is responsible for approximately one third of the driving force during this process.

2. *Lateral Epidermis*: The lateral epidermis migrate and converge dorsally to seal the embryo at the dorsal midline. These cells activate the JNK and the Dpp signaling pathways, which are required for their stereotypical cell behaviours (Kiehart et al., 2017). In particular, dorsal most epidermal cells elongate in the dorso-ventral direction and acquire planar cell polarity evidenced in the organization of cytoskeletal and adhesion components at the leading edge, which is in contact with the amnioserosa. (Lv et al., 2022)

3. *Actomyosin Cable*: This is a supracellular structure formed at the leading edge of the lateral epidermis, providing the necessary tension for the dorsal closure. Non-muscle Myosin II, a molecular motor present in epithelial cells, interacts with the actin filaments to contract this cable. Although biomechanical experiments have shown that the actomyosin cable is under tension (Kiehart et al., 2000; Hutson et al., 2003), the requirement of this force for closure has been challenged by experiments in which the cable is genetically removed and closure occurs normally (Pasakarnis et al., 2016; Ducuing and Vincent, 2016).

4. *Zipping*: This term is used to describe the process of the lateral edges of the embryonic epidermis progressively coming together starting from the anterior and posterior ends or canthi, to

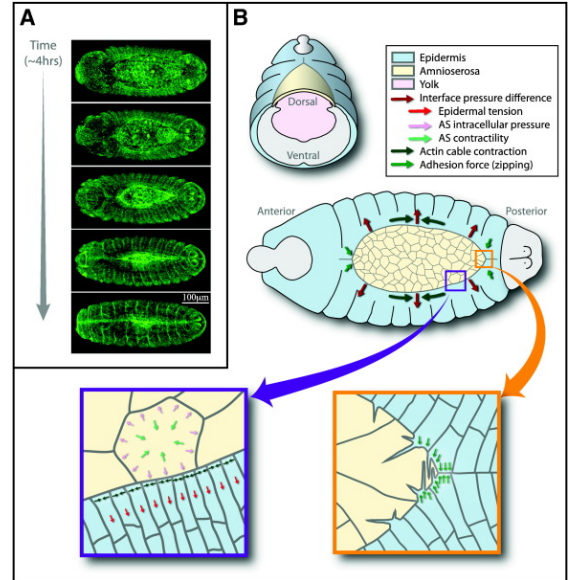


Figure 1: During the process of dorsal closure in an embryo, there is a combination of forces at work. [A] Over a few hours, a gap on the embryo's back gets covered by specific tissue. [B] The forces involved in this process are complex: (1) Forces promoting the closure (green arrows) include the contraction of certain cells and a tangential tension created by a cable of proteins. (2) Forces resisting the closure (red arrows) include tension in the outer layer of the embryo and pressure within certain cells. (3) There are also local forces at the edges of the opening that help seal it (green arrows), like the action of specific cellular structures near the zipping points. The combination of these forces ensures that the opening in the embryo's back gets closed properly (Hayes and Solon, 2017).

close the dorsal surface, much like the way a zipper brings two sides of a garment together. This action, driven by filopodia and lamellipodia from the dorsal most epidermal cells, ensures that closure proceeds in an orderly and efficient manner. Zipping typically starts from the anterior and posterior poles and moves towards the dorsal midline, eventually leading to the complete enclosure of the amnioserosa and the successful completion of dorsal closure (Kiehart et al., 2017).

The interplay between these three components is crucial for dorsal closure. One mathematical model, proposed by Hutson et al. (2003), uses the equation (i) & (ii) from Figure 2. It's important to note that while this equation provides a theoretical model of the forces involved, the exact contribution of each component and how they're regulated during the process of dorsal closure is still an active area of research. Different perturbations can shift the balance between these forces, potentially leading to defects in dorsal closure. However, the process is robust and able to adapt and continue even when key components or forces are compromised. Specifically, laser and genetic experiments show that the dorsal closure system can still function even when one of the primary contributors (amnioserosa, lateral epidermis, or actomyosin cable) is disrupted or removed. For example, when the amnioserosa is removed through laser dissection, dorsal closure initially slows but eventually resumes and completes at a normal rate (Hutson et al., 2003; Peralta et al., 2007). Similarly, when the actomyosin cable is disrupted, a secondary cable forms and enables the pro-

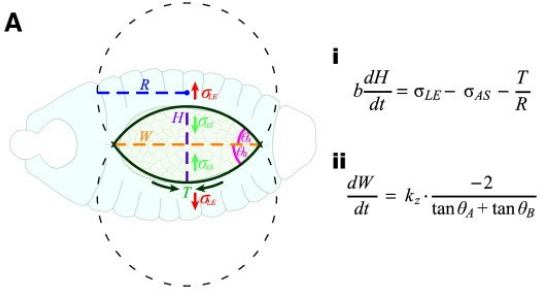


Figure 2: During dorsal closure, the forces involved can be described by simplifying the opening shape into two symmetrical overlapping circular arcs. This allows the closure progression to be represented through two one-dimensional aspects: (i) The alteration in the opening’s height ( $H$ ) is regulated by a balance of forces. This includes the closure-driving contributions from the actin cable (expressed as  $T/R$ ) and the contraction within the amnioserosa (notated as  $\sigma_{AS}$ ) countered by tension in the epidermis that resists closure ( $\sigma_{LE}$ ). The change in height, multiplied by a specific friction coefficient ( $b$ ), helps to describe this balance. (ii) The reduction in the opening’s width ( $W$ ) progresses at a velocity determined by a zipping rate constant ( $k_z$ ), empirically derived, and influenced by the angles at the canthi, referred to as  $\theta_A$  and  $\theta_B$ . This aspect captures how the opening narrows during the process. (Hayes and Solon, 2017).

cess to continue (Rodriguez-Diaz et al., 2008). Even in cases where zipping is prevented, closure still proceeds due to up-regulated forces in the amnioserosa (Peralta et al., 2007). Also, genetic perturbations do not compromise the completion of closure. Closure still completes even when functional Myosin is removed from the purse string (Franke et al., 2005; Pasakarnis et al., 2016), when Myosin activation is blocked (Franke et al., 2005; Duque and Gorfinkel, 2016), and when apoptosis is inhibited (Toyama et al., 2008; Gorfinkel et al., 2009; Muliyl and Narasimha, 2014). These findings show the redundancy in the system, allowing it to adapt and complete dorsal closure despite significant perturbations.

However, despite these layers of redundancy and the robustness of the system, many questions remain. The mechanisms by which the system responds to perturbations, upregulates alternative forces, and ensures successful closure, are not fully understood. The speculation that mechanosensitive mechanisms might play a role in responding to changes in tissue tension is a fascinating hypothesis that warrant further investigation in the balance of these forces (Hunter et al., 2014; Jurado et al., 2016). In this scenario, stress inference may provide a cost-effective way of analyzing tensions in the system and could contribute to the understanding of the mechanosensitive mechanisms underlying the resilience and robustness of the process.

### 3. Methods

Our study focuses on methods for inferring forces from cell geometry, allowing us to determine tensions at cell interfaces and pressures within cells. These are critical parameters that we seek to evaluate through the prism of two fundamental biological forces: **actomyosin contractions** and **cell-cell adhesion** systems (Figure 3). The interplay of these forces affects cell edge length, with actomyosin contractions attempting to decrease it, while cell-cell adhesion tends to extend it (Brodland GW, 2014).

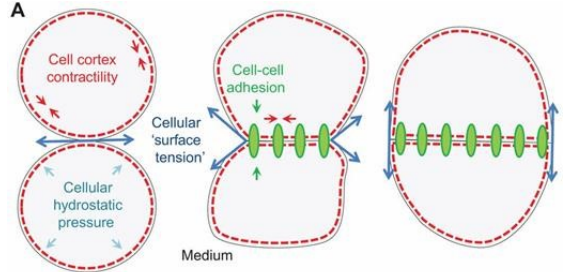


Figure 3: Cell surface tension, adhesion and interfacial tension. Forces acting upon cells in adhesion can be conceptually likened to the surface tension observed in liquids. For individual cells, the so-called cellular surface tension (blue arrows) is governed by the cortical contractile forces, which typically drive the cell towards minimizing its exposed surface area, leading to a rounded cell shape. However, when multiple cells come into proximity, adhesion between them creates counteracting forces that promote cell-cell interactions and increase the contact surface between them. The equilibrium or balance achieved between these contracting and adhesive forces is termed as interfacial tension.(Fagotto, 2014).

In this context, the concept of effective edge tension arises from the interplay of these forces. The simultaneous action of both forces adds layers of complexity, making it challenging to predict the resultant edge behavior. Therefore, an in-depth understanding of the specific system under investigation is crucial for accurate interpretation of the effective edge tension.

Our method works on the fundamental premise of **mechanical equilibrium**, presuming cell shapes result from a balance of interactions among cells. This concept is widely applied in many biological contexts, such as tissue morphogenesis, where cell shapes tend to be static or quasi-static, experiencing a slow progression of near-equilibrium states. Therefore, we employ a **quasi-static** assumption in our models, meaning cellular deformations are assumed to occur slowly, minimizing the impact of viscous forces. Nonetheless, it’s important to recognize that this assumption does not universally apply, and there are situations where tissues significantly deviate from mechanical equilibrium (Roffay et al., 2021).

The concept of equilibrium, suggests that at a vertex where three cell junctions meet under equal tension, angles of  $120^\circ$  form. If the angles deviate from this value, it indicates that junction tensions are different and it is possible to calculate the ratio of tensions for these three cell junctions for the vertex to remain in equilibrium (Fig. 4(a)), and this can be done across the whole tissue. We assign one edge a reference (Fig. 4(b)), or unity, tension to compute the tensions in the other edges. And assuming edge tension constancy, we apply this process to all relevant edges, resulting in a color-coded tension map (Fig. 4(c)).

#### 3.1. Equations

Two-dimensional stress inference, as highlighted in the studies by Ishihara and Sugimura (2012) and Brodland GW (2014), is guided by a couple of crucial principles. These principles, which both rely on the concept of mechanical equilibrium within cellular structures, form the bedrock of the two main equations involved in the process.

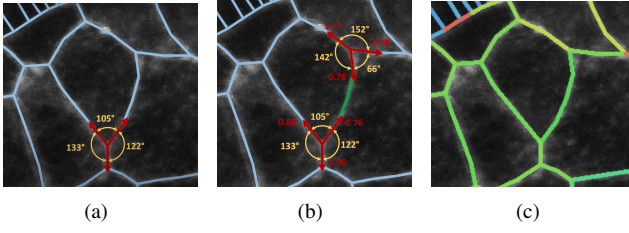


Figure 4: Visualization of cellular tension equilibrium. (a) Three cell junctions meeting at  $120^\circ$  angles under equal tension. Deviations from this angle indicate tension shifts. (b) Assignment of a reference or unity tension to one edge, allowing for the calculation of other tensions. (c) Application of the edge tension constancy across all relevant edges, resulting in a color-coded map representing the tension distribution (Brodland GW, 2014).

### 3.1.1. Force balance

The first principle underscores the force balance of a vertex where three cell junctions meet in a two-dimensional plane. This principle postulates that when the sum of vectors, representing edge tensions, equates to zero, the triple junction remains at rest. With a knowledge of the orientation of the membranes at each vertex  $i$  (hence implying the direction of the force vectors) ( $\tau_{i,\alpha\beta}, \tau_{i,\beta\gamma}, \tau_{i,\gamma\alpha}$ , where  $|\tau|=1$ ), one can infer the relative magnitudes of tensions of edges at a given vertex  $i$  ( $T_{\alpha\beta}, T_{\beta\gamma}, T_{\gamma\alpha}$ ). In a simplified form, the equation for this principle can be represented as:

$$T_{\alpha\beta}\widehat{\tau_{i,\alpha\beta}} + T_{\beta\gamma}\widehat{\tau_{i,\beta\gamma}} + T_{\gamma\alpha}\widehat{\tau_{i,\gamma\alpha}} = 0 \quad (1)$$

In terms of directions, the forces due to cell edge tensions along the x and y-axis are balanced at each vertex (Fig. 5(a)). These balanced forces yield two equations per triple junction, namely:

$$T_1 \cdot \cos(\phi_1) + T_2 \cdot \cos(\phi_2) + T_3 \cdot \cos(\phi_3) = 0 \quad (2)$$

$$T_1 \cdot \sin(\phi_1) + T_2 \cdot \sin(\phi_2) + T_3 \cdot \sin(\phi_3) = 0 \quad (3)$$

These equations encapsulate the balance of tensions around the edge. A critical assumption that underpins this equilibrium condition is that the membrane tensions are constant across each interface.

This assumption allows the inference of the relative magnitudes of membrane tensions across an entire (connected) tissue. The reason we describe these tensions as "relative" is rooted in a geometric analogy: similar to how innumerable triangles can be constructed to fit a particular set of three angles without determining their exact side lengths, the tensions we infer are comparative in nature, not definitive absolute values.

### 3.1.2. Young-Laplace law

In the examination of epithelial structures *in vivo*, it is evident that apical cell membranes often exhibit curvature, which is largely attributable to differences in apical pressures between adjacent cells forming an edge. These apical pressures encompass all isotropic stresses acting across a cell's interfaces, such as the isotropic action of apicomедial actomyosin.

Assuming a simplification of constant tension across interfaces (Fig. 5(b)), these membrane curvatures can be approximated as following the path of a circular arc, marked by a defined radius of curvature ( $R_{\alpha\beta}$ ) and an associated circular centroid. This allows for the inference of differential pressure via the Young-Laplace law, which states that the pressure difference between two cells is equal to the tension along the interface divided by the radius of curvature:

$$\Delta P = p_\alpha - p_\beta \quad (4)$$

$$p_\alpha - p_\beta = T_{\alpha\beta}/R_{\alpha\beta} \quad (5)$$

Together, these principles form the set of mechanical balance equations, one for each triple junction (balancing the interface tensions) and another set derived from the Young-Laplace equation for each cell (balancing the intracellular pressures). These equations, when applied in reverse, starting from the observed equilibrium cell shapes, allow to deduce the underlying cell interface tension and cell pressure.

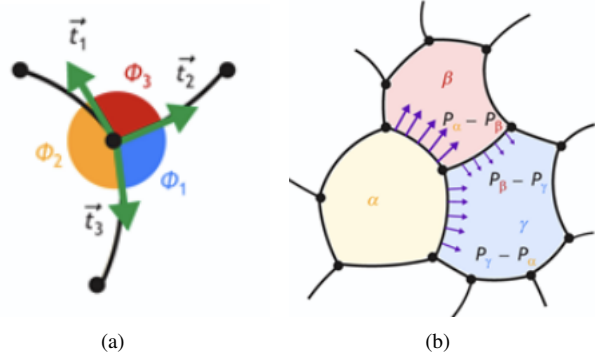


Figure 5: (a) Representation of the tension vectors at each node is shown, accompanied by their respective angles  $\phi$ . The magnitude of tension is the same at both ends of the edge. (b) Representation of cellular pressures. Each cell, labelled  $\alpha, \beta$  or  $\gamma$ , is assumed to have a homogeneous pressure  $P$ .

### 3.2. Inference strategies

Relying on the physical assumptions previously discussed, various inference strategies have been developed to estimate relative junctional tensions and cellular pressures. These strategies frame force inference as an over-determined problem. Specifically, there are fewer interfacial tensions than the sum of the force balance equations' x and y components, and the number of cells (or pressures) is less than the edges (or curvatures). For computational efficiency, they assume uniformity in interfacial tensions along each edge and uniformity in intracellular pressures. Force inference methods strive to find the closest match between estimated tensions and observed data. Different approaches share the common goal of achieving the "best fit."

In this analysis, we focus on two force inference strategies: (i) Cellular Force-Inference Toolkit (CellFIT) (Brodland GW, 2014); and (ii) Dynamic Local Intercellular Tension Estimation (DLITE) (Vasan et al., 2019).

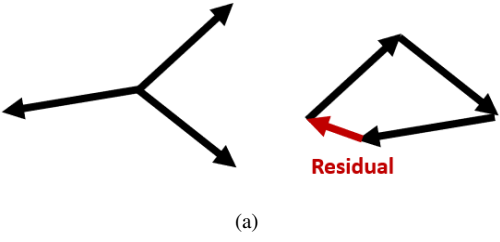


Figure 6: A schematic of a tension residual (for a given vertex). Rearranging the force vectors, residuals are conceptualised as the deviation from a closed triangle

### 3.2.1. CellFIT

The CellFIT method defines the "best fit" as the distributions of tensions (or pressures) that minimize the sum of the squared residuals of each force balance (or Young-Laplace) equation. For estimating tensions, the differences (referred to as residuals,  $b_i^T$ ) represented in Figure 6 are calculated with a specific formula (Equation 6).

$$b_i^T = T_{\alpha\beta}\widehat{\tau_{i,\alpha\beta}} + T_{\beta\gamma}\widehat{\tau_{i,\beta\gamma}} + T_{\gamma\alpha}\widehat{\tau_{i,\gamma\alpha}} \quad (6)$$

A similar process is used for pressure, residuals ( $b_\alpha^p$ ) are defined as:

$$b_\alpha^p = p_\alpha - p_\beta - T_{\alpha\beta}/R_{\alpha\beta} \quad (7)$$

The objective of tension inference is to minimize:

$$\varepsilon_T^{CellFIT} = \sum_i \|b_i^T\|^2 \quad (8)$$

Meanwhile, pressure inference aims to minimize:

$$\varepsilon_p^{CellFIT} = \sum_\alpha \|b_\alpha^p\|^2 \quad (9)$$

Constraints are applied during the minimization process to prevent meaningless solutions where all tensions and pressures are zero, and to establish the scale of the solution since the inferences are relative.

For tension minimization, the constraint is that the mean tension should equal 1:

$$\sum_{\alpha\beta} T_{\alpha\beta} = n_e \quad (10)$$

For pressure minimization, the constraint is that the mean pressure should equal 0:

$$\sum_\alpha P_\alpha = 0 \quad (11)$$

These constraints guarantee that the results of the methodology are relevant and properly scaled.

#### a) Tension inference in CellFIT

In CellFIT, tension inference is seen as a matrix inversion problem. There are  $2n_v$  force balance equations, taking into account both the x and y components of force balance across  $n_v$

vertices. These equations are arranged as rows in a matrix, referred to as  $G_T$ , with dimensions of  $(2n_v \times n_e)$ . Each pair of rows considers force balance at a given vertex: elements are either (i)  $\widehat{\tau_{i,\alpha\beta}} \cdot \widehat{e_x}$  on even rows and  $\widehat{\tau_{i,\alpha\beta}} \cdot \widehat{e_y}$  on odd rows for edges connected to that vertex, or (ii) 0 for edges that are not. Consequently, these  $2n_v$  force balance equations can be translated into a problem solved through linear algebra.

$$G_T T = 0 \quad (12)$$

Here,  $T$  is an  $(n_e \times 1)$  matrix, considering the tensions of each of the  $n_e$  edges.

A least-squares calculation is performed using the pseudo-inverse  $G'_T G$ , given that the system of equations is over-determined:

$$G'_T G T = G^T 0 = 0^* \quad (13)$$

Here,  $G'$  represents the transpose of matrix  $G$ , and  $0^*$  is an  $(n_e \times 1)$  matrix. The constraint is introduced by utilizing a Lagrange multiplier, denoted as  $\lambda_T$ .

$$\begin{pmatrix} G'_T G & C'_T \\ C_T & 0 \end{pmatrix} \begin{pmatrix} T \\ \lambda_T \end{pmatrix} = 0 \quad (14)$$

where  $C_T$  is the constraint matrix ( $C_T = (1, 1, \dots, 1)$ , an  $(n_e \times 1)$  matrix). numpy's `linalg.lstsq` function is used to perform a least-squares minimisation

#### b) Pressure Inference in CellFIT

CellFIT executes a least-squares minimization on a system of Young-Laplace equations. Tensions from the above minimization are used as a fixed input. This is framed, similarly to above, in terms of a matrix equation:

$$G_p p = q = \begin{pmatrix} \frac{T_1}{R_1} \\ \frac{T_2}{R_2} \\ \vdots \\ \frac{T_{n_e}}{R_{n_e}} \end{pmatrix} \quad (15)$$

Here,  $G_p$  is an  $(n_e \times n_c)$  matrix, with each row representing a Young-Laplace equation. The equation takes values of -1, 0, or +1. +1 represents the convex cell, -1 the concave cell, and 0 signifies non-involved cells.

As with tension inference, Lagrange multiplier constraints are imposed:

$$G'_p G p = G'_p q \quad (16)$$

$$\begin{pmatrix} G'_p G_p & C'_p \\ C_p & 0 \end{pmatrix} \begin{pmatrix} p \\ \lambda_p \end{pmatrix} = \begin{pmatrix} G'_p q \\ 0 \end{pmatrix} \quad (17)$$

Here,  $C_p = (1, 1, \dots, 1)$  is an  $(n_c \times 1)$  matrix.

### 3.2.2. DLITE

DLITE (as described by Vasan et al. (2019)) works on the same basic ideas as CellFIT. Both methods make the same assumptions about the forces at each point and how they comply with the Young-Laplace law at each edge. However,

DLITE is different from CellFIT in three key ways: (i) instead of constraining the mean tension, DLITE uses a regulariser term that penalises small tensions at each vertex; (ii) due to the non-linearity in the regulariser term, fitting is solved through minimising a cost function; and (iii) the initial guess of said cost function is derived from the inferred tensions and pressures in the previous frame. CellFIT and DLITE however remain similar in terms of their variational nature, solving tensions first, and pressures next, using inferred relative tensions as fixed inputs.

#### a) Tension inference in DLITE

Tensions are inferred by minimising the following cost function:

$$\varepsilon_T^{DLITE} = \sum_i^{n_v} \left[ \sum_{\alpha\beta \in i}^{n_e \in i} T_{\alpha\beta} \widehat{\tau}_{i,\alpha\beta} \cdot (\widehat{e}_x - \widehat{e}_y) \left( 1 + \frac{1}{\sum_{\alpha\beta \in i}^{n_e \in i} T_{\alpha\beta}} \right) \right] \quad (18)$$

where  $\sum_{\alpha\beta \in i}^{n_e \in i} T_{\alpha\beta}$  is the regulariser.

For the initial frame, we start the minimization process by employing random estimations of tension, sourced from a uniform distribution  $T_{init} \sim U[0, 1]$ . Subsequent frames then utilize the inferred tension from the preceding frame's identical edge as their starting point. If an edge doesn't appear in the prior frame, we compute the initial tension guess by averaging the tensions from the previous frame's edges linked to the adjacent vertices. In situations where none of these edges appear in the former frame, a random estimation is made in the same manner as for the first frame.

The minimisation is constrained such that the minimum tension is 0. And is solved with *scipy.optimize.minimize* using the *L-BFGS-B* method.

#### b) Pressure inference in DLITE

Pressures are inferred by minimising a cost function too. This is defined by:

$$\varepsilon_p^{DLITE} = \sum_{\alpha\beta}^{n_e} p_\alpha - p_\beta - T_{\alpha\beta}/R_{\alpha\beta} \quad (19)$$

Note that this is identical to the function being minimised by CellFIT. The key difference is that a minimiser is used, rather than deploying matrix inversion. In principle, both should yield similar results, if seeded with the same tensions.

$T_{\alpha\beta}$  values are those generated from the above minimisation. Like with tension inference, the initial guess of the first frame is seeded with a random guess dictated by  $p_{init} \sim U[0.5, 0.5]$ . Subsequent frames either adopt pressures from the preceding frame's corresponding cells or, in their absence, use averaged pressures from neighboring cells. When no previous frame reference exists, a random guess serves as the starting point.

### 3.3. Comparative between DLITE and CELLFIT

In the exploration of cell tension and tissue morphology, the comparative understanding between DLITE and CELLFIT results, as demonstrated in Vasan et al. (2019), is essential. This

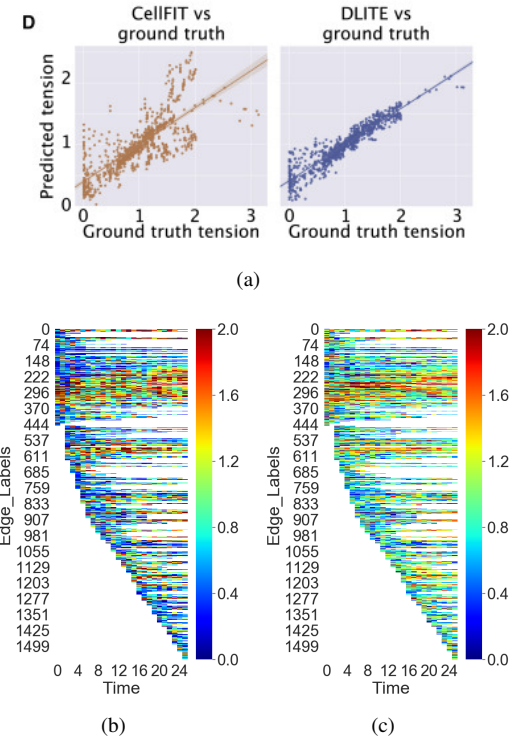


Figure 7: (a) A comparison of inferred versus ground-truth tensions for CellFIT ( $r = 0.75$ ) and DLITE ( $r = 0.94$ ). Where,  $r$  is the Pearson's correlation coefficient (Vasan et al., 2019). A heat map of dynamic edge tensions from the amnioserosa, predicted by CellFIT (b) and DLITE (c), with standard deviations of 0.79 and 0.55, respectively.

comparison is particularly detailed for synthetic data, where cells are generated from random Voronoi tessellations and morphed to minimum energy configurations, allowing ground truth tensions to be known. This unique environment supports the comparative analysis of these two methodologies, offering insights that have broader applications.

The results in Vasan et al. (2019) clearly articulate the differences between the two approaches (Figure 7(a)). For individual frames, both methodologies yield similar outcomes. However, CELLFIT proves to be more efficient and easier to implement. Its advantage lies in the elimination of the need for tracking each edge and cell over time, making it a more streamlined solution for isolated time points. On the other hand, DLITE, emerges with significant advantages in various conditions. The robustness, increased performance across time points, stability in handling segmentation challenges, and adaptability with limited experimental data sets provide DLITE with a more comprehensive and versatile solution (Vasan et al., 2019).

To compare the performance of CELLFIT and DLITE in the context of our data, we inferred cell tensions in the amnioserosa of a single embryo over 25 frames encompassing 50 min of dorsal closure. Our observations, depicted in Figures 7(b) and 7(c), demonstrate the inferred tensions at each cell interface. Notably, CELLFIT's results display noticeable fluctuations in the standard deviation ( $std=0.79$  compared to DLITE's 0.55), indicating higher variability in tension estimations. Conversely,

DLITE's consistency is evident, marked by its smooth tension inference across different time intervals, allowing for sequential tension inferences in films. Such consistency facilitates a robust comparative analysis of tissue properties across different timeframes. While DLITE's resilience stands out in multi-frame analysis, CELLFIT remains invaluable for dissecting individual frames, even when faced with segmentation challenges.

### 3.4. Image Analysis and Deep Learning in Tissue Segmentation

Time-lapse movies of Drosophila embryos during dorsal closure have been obtained in the lab. These embryos carry the endogenous ECadherin gene (a component of adherens junctions) fused to the coding sequence of the green fluorescent protein. This fusion facilitates the visualization of apical cell membranes in all epithelial cells. In these recordings, between 20 and 25 z-sections,  $1.5\mu\text{m}$  apart, were collected every 2 minutes.

In our study, we use the maximum intensity projection to transform the 3D information of the tissue into a 2D representation. An important consideration when using this 2D representation is the assumption that the tissue under study is planar. Although the amnioserosa has a generally flat shape in the central region, it exhibits an elliptical dome shape, causing the sides to fall out of the 2D plane. This assumption results in a loss of spatial information related to the shape of the amnioserosa, particularly in the lateral regions.

The successful implementation of computational models such as CellFIT and DLITE necessitates an accurate and reliable representation of the cellular tissue under investigation. To this end, we have used different image analysis techniques and deep learning algorithms to perform precise tissue segmentation and cell tracking.

#### a) Image Pre-Processing and Noise Reduction

The primary challenge in image preprocessing was the removal of non-specific background noise from the maximum intensity projection, primarily attributed to yolk and sub-amnioserosa embryonic components. To get rid of this background (Figure 8A), a custom-developed algorithm was designed (GitHub link) to select a region in the z-plane encapsulating the maximum projection in both the X and Y axes. The intersection of these projected areas delineated a volume corresponding to the noise originating from within the embryo. By excising this volume, the algorithm effectively minimized the interference of background elements and enhanced the clarity of the tissue of interest, as we can see in Figure 8B, thereby streamlining subsequent analyses.

#### b) Tissue Segmentation and Cell Tracking via Deep Learning

Following noise reduction, this work made use of an advanced deep learning-based program known as "Tissue Analyzer" (Aigouy et al., 2016). Tissue Analyzer is proficient in accurately delineating cell boundaries within the tissue - a crucial step in understanding the spatial dynamics of the amnioserosa.

By deploying a set of deep learning algorithms, Tissue Analyzer was able to segment individual cell boundaries with high precision, laying the groundwork for subsequent analysis. It is essential to note that Tissue Analyzer is designed with a manual

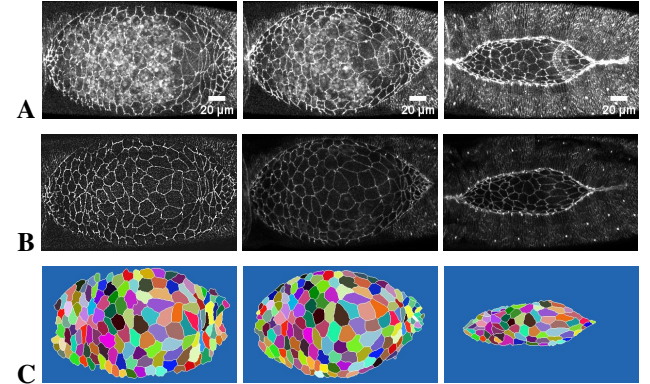


Figure 8: The figure consists of three panels A, B and C. Within each panel, three images represent the distinct phases of the amnioserosa's development in a wild-type embryo. Using the moment of closure as the reference point (time zero), the images depict the early stage at -156min, the mid-stage at -120min, and the late stage at -52min. Panels A and B display the amnioserosa in two forms: unprocessed images from maximum projection and post-processed images with noise from confocal captures removed. Panel C presents the segmented and tracked cells over time.

correction method which is often required to ensure accuracy, thereby laying the groundwork for subsequent analysis. Furthermore, Tissue Analyzer is equipped with features facilitating cell boundary tracking over time. This capability enables the study to monitor changes in cell shape, size, and interaction, providing a dynamic view of amnioserosa cell behaviour throughout the course of the investigation.

### 3.5. Examined Genotypes

In our endeavor to understand the forces at play in the dynamics of dorsal closure, we have specifically analyzed a set of genotypes, ranging from essentially wild-type embryos to those with modulated Myosin II activity.

1. *ECadherin-GFP* (Control): This strain serves as a control, equipped with a green fluorescent protein (GFP) fused to E-cadherin, an essential adhesion protein. This modification allows for visualization and tracking of E-cadherin during dorsal closure through confocal microscopy, providing a baseline for normal cell-cell adhesion and tension dynamics (Figure 9(a)).

2. *AS-GAL4, ECadherin-GFP/UAS-MbsN300*: Making use of the GAL4/UAS system that allows the ectopic expression of genes of interest in specific tissues, in these embryos, a constitutive active form of a Myosin phosphatase is ectopically expressed in the whole amnioserosa, allowing to analyze the mechanics of the tissue when Myosin activity is reduced. (Figure 9(b)).

3. *prd-GAL4, ECadherin-GFP/UAS-NLSmCherry, UAS-MbsN300*: In these embryos, Myosin activity is reduced in groups of cells in the amnioserosa (these cells are also labeled with a Red Fluorescent Protein directed to the nucleus through a nuclear localization signal), generating a mosaic tissue where some cells have reduced Myosin activity and other cells have normal Myosin activity (Fig. 9(c)).

By studying these genotypes with alterations in myosin levels, we can expect different patterns of inferred tension within amnioserosa cells.

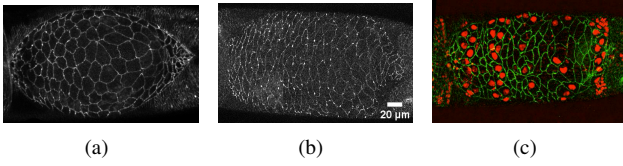


Figure 9: Depicted are frames from different genotypes: (a) represents the control (ECadherin-GFP), (b) displays the reduced myosin genotype (AS-GAL4, ECadherin-GFP/UAS-MbsN300) in early stages, and (c) illustrates the striped reduced myosin embryo (prd-GAL4, ECadherin-GFP/UAS-NLSmCherry, UAS-MbsN300 ).

#### 4. Results and Discussion

We initiate our results section with an exploration of the network of cellular forces during early dorsal closure in Drosophila embryos between the Amnioserosa (AS) and the Lateral Epidermis (LE). Our goal here is to validate our methodology against the analysis presented in Brodland GW (2014). By replicating their analysis, we aim to ensure the robustness and accuracy of our method. Beyond this replication, our investigation evolves to analyze tension distributions within ECadherin-GFP (control) embryos throughout the closure process, offering a nuanced perspective on force orchestration within the amnioserosa tissue. Finally, we analyze genetically perturbed embryos in which Myosin II activity is reduced in the whole amnioserosa (AS-GAL4, ECadherin-GFP/UAS-MbsN300) or in groups of cells (prd-GAL4, ECadherin-GFP/UAS-NLSmCherry, UAS-MbsN300). Our aim is to explore how the balance of junctional tensions within the tissue changes when the main force generator motor is affected.

##### 4.1. Dorsal Closure Dynamics

To validate our implementation of CELLFIT, we utilized fluorescence images of the Amnioserosa/Lateral Epidermis (AS/LE) boundary, which were previously examined in Brodland GW (2014) (Figure 10(a)). This facilitated a direct comparison with our findings. Additionally, we expanded our investigation by analyzing a new fluorescence image captured from a different embryo, yet within a spatial framework similar to the original (Figure 11).

Comparing the tension maps from Brodland GW (2014) (Figure 10(b)) with the ones obtained by our segmentation and CellFIT inference method (Figure 10(c)), we noticed noteworthy differences. First, we observed that the pressures are exceedingly variable with no apparent pattern. We attribute these changes mainly to segmentation errors, which led us to decide not to analyze these pressures further in the next experiments. The potential implications of this will be further discussed in the concluding remarks section. Then, we observed that junctional tensions are not exactly the same, and these variations are more pronounced in certain regions (indicated by black arrows in 10(c)).

In spite of these differences, our analysis shows a clear distinction between the tension within the amnioserosa (AS/AS) and those within the lateral epidermis (LE/LE) (Figure 10(d)) (Figure 11(b)), in line with the observations from Brodland GW (2014).

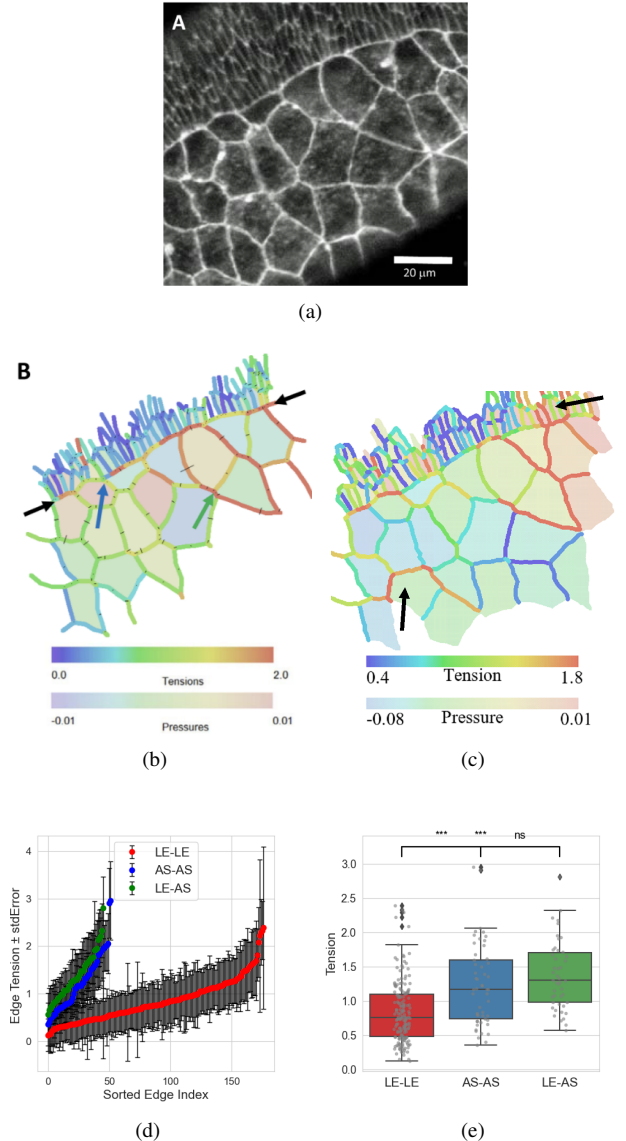


Figure 10: CellFIT Analysis During Early Dorsal Closure in a Living Drosophila Embryo at the LE/AS Boundary. (a) Original fluorescence image analyzed in CellFIT results. (b) Tension map from CellFIT paper. (c) Tension map obtained by our segmentation and CellFIT inference method. (d) Differentiation into three edge categories: AS/AS, LE/LE, and LE/AS, displaying tensions along with standard error across these edges. (e) Boxplot representing tensions in the three categories, highlighting statistically significant differences.

Specifically, we found a marked two-fold difference in these tensions, indicating a fine balance of forces within the tissue. These results are consistent with a scenario in which the ventrally directed forces in the closely packed epidermis are counterbalanced by the dorsally directed forces generated within the amnioserosa. In a situation of mechanical equilibrium, the cell junctions in the amnioserosa, which are fewer and more widely spaced bear more tension than the more abundant and closely packed cell junctions of the lateral epidermis.

However, in contrast to the findings from Brodland GW (2014), which postulate that higher tensions in the LE/AS interface are influenced by shear forces at work within the tissue,

our study does not clearly demonstrate these pattern, either in our replication of the CellFIT analysis (Figure 10(e)) or in our new data (Figure 11(c)). This deviation from the expected results requires further investigation.

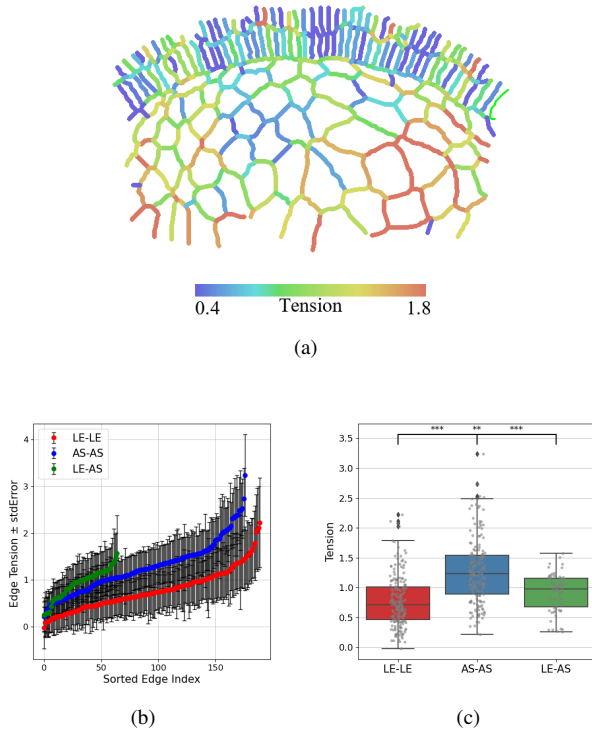


Figure 11: CellFIT Analysis of Early Dorsal Closure in a Living Drosophila Embryo at the LE/AS Boundary. (a) Tension map of a fluorescence image obtained in a similar spatial framework. (b) Tension map obtained by our segmentation and CellFIT inference method. (d) Differentiation into three edge categories: AS/AS, LE/LE, and LE/AS, displaying tensions along with standard error across these edges. (c) Boxplot representing tensions in the three categories, highlighting statistically significant differences.

Within the amnioserosa, an additional layer of complexity is evident. The tensions at the cell interfaces exhibit substantial variability. This finding aligns with the known local dynamic contractions of the cells in this tissue. Having established this complex picture of cellular tensions within a small framework of the tissues that play a role in the dorsal closure, we now turn our attention to an investigation of the amnioserosa in different genotypes.

#### 4.2. Tension Inference in the Amnioserosa over Dorsal Closure

Building upon our prior CELLFIT validation, we proceeded to apply DLITE to time lapse movies of control embryos. We performed stress inference using DLITE on one time lapse movie of dorsal closure, but restricted our further analysis to individual frames corresponding to three representative dorsal closure stages, early, mid and late.

Our findings have revealed a consistent pattern: larger cells within the amnioserosa tend to experience higher levels of tension in early and mid dorsal closure stages, as evidenced by a coefficient of Pearson  $r=0.56$  with a  $p$ -value of  $4e-13$  (see Figure 12B). Intriguingly, these larger cells are often situated

centrally within the amnioserosa. We present this tension distribution visually, through a heatmap (Fig. 12C), providing a clear depiction of tension distribution across cells of varying sizes. We observe that this correlation ( $r=-0.12$ ,  $p=0.32$ ) is lost in later dorsal closure stages.

We propose that the higher tension observed in central cells is the result of the ventrally directed pulling from the lateral epidermis. As described in Section 2, the amnioserosa in dorsal closure can be simplified into two symmetrical overlapping circular arcs which describes its elliptical shape. If we decompose the ventrally directed forces exerted by the lateral epidermis into its X and Y components along the whole circular arc, we can observe that the dorsoventral component in the central region is higher than in more lateral regions of the amnioserosa. Assuming the amnioserosa exhibits viscoelastic behaviour, the continuous pull of the lateral epidermis would generate a creep<sup>1</sup> response in the amnioserosa, which manifest itself in the expansion of the central cells and higher tension along its junctions.

We further explored our tension maps by analysing the relationship between cell junctional tension and orientation. The orientation of cell junctions was set relative to the antero-posterior and dorso-ventral axis of the embryo and the corresponding length and tension are shown in the polar plots in Figure 12D. During early and mid dorsal closure stages, cell junctional tensions were similar across all orientations. However, during late dorsal closure stages, we observed an increase in tension as well as in length along the horizontal axis, corresponding to the anteroposterior axis of the embryo, revealing a change in the balance of tensions within the amnioserosa as dorsal closure progresses.

We hypothesize that as the process nears its conclusion, the dorsoventral resistance from the lateral epidermis diminishes in its role. Concurrently, the forces generated along the antero-posterior axis gain prominence, resulting in an equilibration of tensions throughout the tissue. This emphasis on the antero-posterior forces, driven by more intricate developmental mechanisms, represents a key mechanical adaptation in the terminal phases of dorsal closure, which would facilitate the pulling together of the edges to ensure closure.

Finally, we measured the correlation between the number of cell edges and their corresponding tension, with the idea to test that an increased number of edges might distribute tension more evenly, thereby reducing individual edge tension. There was no significant correlation ( $r=0.12$  pearson correlation) between the number of cell interfaces and their corresponding tensions. Such findings suggest that the cells within the amnioserosa, and biological systems in general, often exhibit complexities that challenge our preliminary expectations.

#### 4.3. Tension Inference in the Amnioserosa with reduced Myosin activity (AS-GAL4, ECadherin-GFP/UAS-MbsN300)

By employing stress inference methods on the early stage of the AS-GAL4, ECadherin-GFP/UAS-MbsN300 genotype em-

<sup>1</sup>Creep refers to the time-dependent deformation of a material when subjected to a constant load or stress. This behavior is observed in materials with viscous properties.

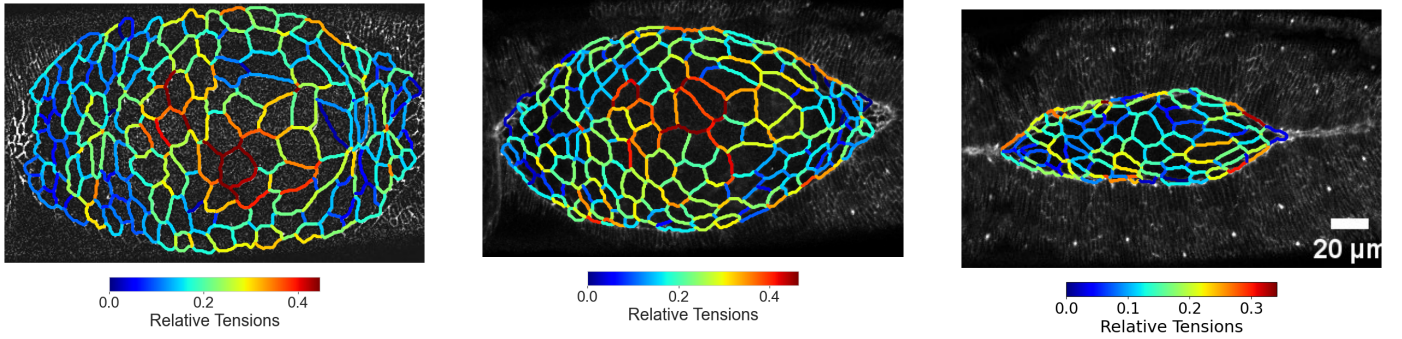
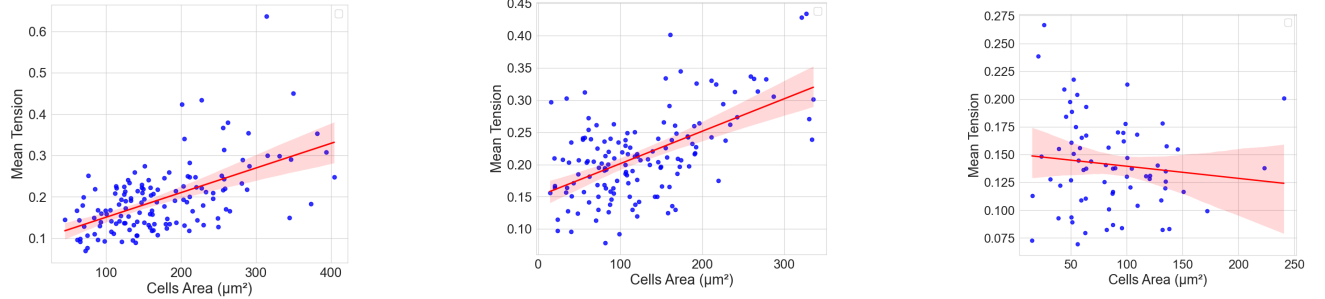
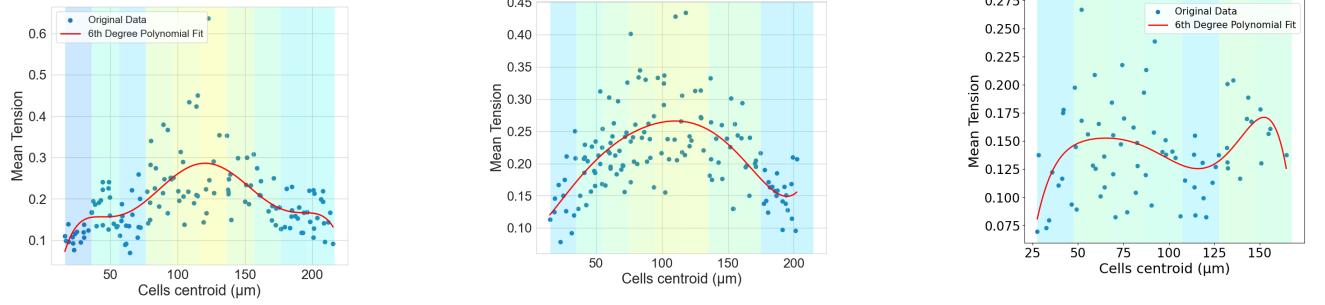
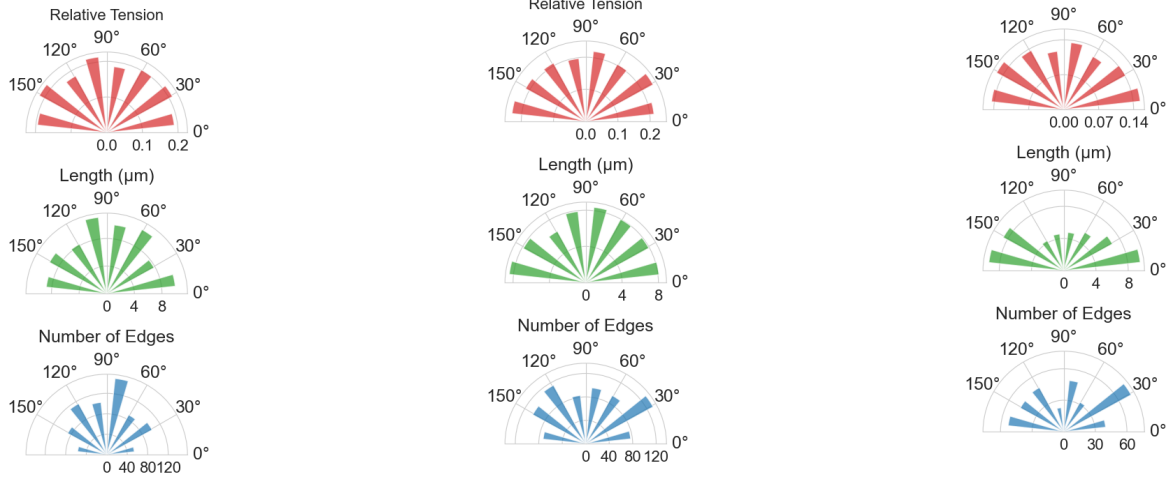
**A****B****C****D**

Figure 12: Comprehensive analysis of cellular tensions within a living Drosophila embryo's amnioserosa across three key developmental stages: early (-156min), mid (-120min), and late (-52min) stages, with the point of closure serving as time zero. Columns represent these respective stages. (A) Relative tension map overlaid on a filtered image, visualizing the spatial distribution of inferred tensions by DLITE. (B) Plots representing the relationship between mean cellular tensions and cellular area for each of the three time stages. The coefficient of Pearson  $r$  measures the linear correlation between the variables. For early stage,  $r=0.56$ ,  $p=4.5e-13$ ; for mid stage,  $r=0.57$ ,  $p=2.0e-13$ ; for late stage,  $r=-0.12$ ,  $p=0.32$ . The accompanying  $p$ -values indicate the statistical significance of each correlation. (C) Illustration of the distribution of mean cellular tensions along the x-axis, providing insights into tension alignment. (D) Polar plots showcasing the distribution of tension, edge length, and the number of edges according to their orientation for each of the three distinct time stages. The plots provide a visual representation of the anisotropy and orientation preferences in the tension, length, and number of cellular edges at each time stage.

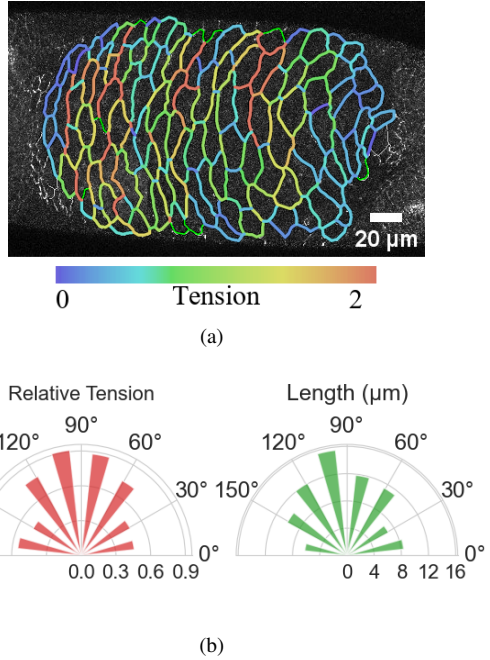


Figure 13: Analysis of the amnioserosa in a genotype AS-GAL4, ECadherin-GFP/UAS-MbsN300 Drosophila embryo with reduced myosin during its early stage. (A) A relative tension map is overlaid on a filtered image, illustrating the spatial distribution of inferred tensions as determined by CELLFIT. (B) Polar plots depict the distribution of tension and edge length according to their orientation. These plots offer a comprehensive visual insight into the anisotropy and orientation preferences concerning the tension and length of cellular edges.

bryo, as depicted in Figure 13, we delved into the characteristics of cells in which Myosin activity is reduced. Specifically, we observe that cells are larger and more elongated in the dorso-ventral axis (Figure 13(a)) than control embryos (Duque and Gorfinkiel, 2016). Interestingly, tensions are higher in dorsoventral junctions than in anteroposterior junctions, a trend that is further illustrated in Figure 13(b). In agreement with this observation, we detected a significant positive correlation ( $r=0.85$  pearson corr.) between edge length and tension.

Thus, our observations show that cells with reduced Myosin activity show larger size, more elongated shape in the dorsoventral direction, and higher junctional tension in dorsoventral edges relative to anteroposterior edges. We surmise that this response is a consequence of their diminished ability to resist the pulling forces of the lateral epidermis due to their weakened contractile potential. This highlights a pivotal role of Myosin, not only in the generation of force, but also in preserving cell structure in cell faced to strenuous morphogenetic forces.

#### 4.4. Tension Inference in Mosaic Amnioserosa with Heterogeneous Myosin activity (prd-GAL4, ECadherin-GFP/UAS-NLSmCherry, UAS-MbsN300)

We further explored the influence of Myosin II in the distribution of tension within the amnioserosa by analysing the amnioserosa of embryos in which Myosin II activity was reduced in a mosaic manner, i.e. in dorsoventral stripes of cells. In these embryos, the cells with reduced Myosin II activity are also labeled with a red fluorescent protein that localizes to the

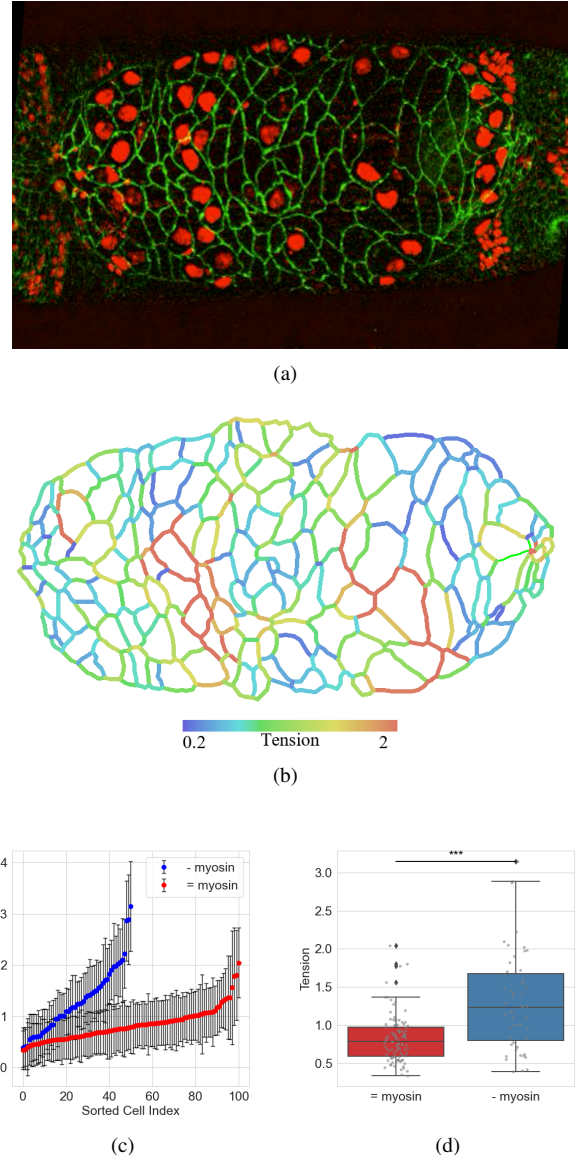


Figure 14: Analysis of the prd-GAL4, ECadherin-GFP/UAS-NLSmCherry, UAS-MbsN300 genotype in dorsal closure. (a) Microscopic view of the amnioserosa in which Myosin activity was reduced in a mosaic manner, labeling the modified nuclei with a red fluorescent protein. (b) CellFIT distribution of tensions visualized from the imaging data. (c) Differentiation between the muted-myosin cells and normal cells, with a display of tensions along with their standard error across the edges within these categories. (d) Boxplot representation of the tensions within the two categories, underscoring the statistically significant differences between them.

nucleus, clearly visualized in Fig. 14(a). As expected, these cells were discernibly larger than those with normal myosin activity. This variance in cell size can be attributed to the pivotal role of Myosin II in cellular contractility. Essentially, myosin governs tension within the cell's cortex, thereby influencing its size and shape. When there's a decrease in myosin concentration, cells exhibit reduced contractility, which manifests as an expansion in their size.

Further analysis, especially from the data in Figure 14(d), revealed that these enlarged, myosin-depleted cells registered a

statistically significant increase in tension. At first glance, this might appear contradictory, given that myosin is traditionally recognized as a primary source of contractile force. However, this increased tension can be influenced by the neighboring cells with normal myosin levels. Essentially, these cells with their typical contractile capabilities exert a pull on the myosin-depleted cells, intensifying the tension at their interfaces, reminiscent of the observations in the reduced myosin genotype. Interestingly, we have observe an accumulation in the myosin II at these interfaces (data not shown). This behavior is consistent with the known tendency of myosin to concentrate at the boundaries of cells that are subjected to mechanical stress, as corroborated by (Sumi et al., 2018).

#### 4.5. Methodological Considerations and Limitations

The investigation into relative tension maps within the cells of the amnioserosa in wild-type and various genotypes has allowed us to discover tension heterogeneities within the tissue. This exploration, while promising, raises questions about the validity and reliability of our mathematical inferences. Specifically, as we demonstrated in our first result replicating the CellFIT experiment, even using the same image, our tension outcomes were slightly different, while the inferred pressures showed a more considerable variation.

The first consideration we must address is that the application of mathematical models for stress inference necessitates certain assumptions that could potentially introduce bias. By considering the tissue as quasi-static, we are inherently assuming that viscous forces are negligible over small timescales. This simplification, while facilitating the application of mechanical equilibrium principles, might not truly capture the dynamic nature of cellular forces within the tissue. In particular, the rapid intracellular contractions that the amnioserosa cells undergo present a significant aspect that may be overlooked by our assumptions, potentially leading to imprecise inferences.

The second consideration takes into account that even from the same image, different results can emerge. Building on this idea, our findings confirm that the quality of segmentation critically influences stress inference. The location of nodes, variations in angles, noise, and other irregularities significantly affect inference. Given that ECadherin fluorescence capturing membrane structures is not always a single line of pixels, and the fact that cells are not perfect polyarcs, segmentation can deviate considerably from the actual cellular structure. Furthermore, the conversion of 3D tissue into a 2D representation ignores inherent spatial characteristics, contributing to a potential disparity between the inferred and actual mechanical properties. These complexities of segmentation, combined with the inherent challenges of a mathematical approach, make the validation of our inferences a priority.

An additional challenge arose in our attempt to infer pressures within the cells of the amnioserosa tissue. The pressures are inferred through cell curvature, a process that faced difficulties due to the oscillatory nature and the irregularities and anomalies within the non-uniform curvature of the amnioserosa. These irregularities, along with the complex dynamics of the cells, meant that conventional methods yielded incon-

sistent and inconclusive results regarding pressures. This lack of consistency underpinned our decision not to include pressure analysis in our results, highlighting the need for future research to develop methodologies that can more accurately capture these complex dynamics.

To understand the variability in stress inference, as has been explored in methodologies like Brodland GW (2014) and Vasan et al. (2019), it would be valuable to explore sensitivity analyses, such as minor variations in nodes or edge angles, and examination of the force inference sensitivity to border cells. These considerations intertwine with the continuous segmentation of a time-lapse movie, which presents unique challenges, especially in cell tracking. Mistakes in tracking, delamination of cells, confusion between edges, or complications during cell replication can greatly affect the outcomes. These tracking errors contribute to the variability in tension distributions observed between different frames of a movie, leading to potential inconsistencies in the overall analysis.

From the challenges and intricacies outlined, it's evident that our approach to understanding biomechanics within the amnioserosa is just the beginning. Emphasizing experimental validation, such as laser ablation or the use of fluorescent tension sensors like Vinculin, will be crucial. Furthermore, the evolution and refinement of inference methods to factor in the abrupt and complex cellular changes is a clear imperative for future studies. These steps will be instrumental in refining our understanding and taking our analyses to the next level of accuracy.

## 5. Conclusions

In this Master's thesis, we have explored the cellular force dynamics of the amnioserosa, a vital tissue in dorsal closure in *Drosophila* embryos. To accomplish this, we utilized sophisticated image analysis techniques and computational methods, enabling us to apply non-invasive tension inference. The tension-inferred model was applied under mechanical equilibrium assumptions within the tissue, a model validated using synthetic data.

Our application of this model to experimental amnioserosa tissue during dorsal closure has provided the following results: We demonstrate that cells in the lateral epidermis endure less stress than those in the amnioserosa. Additionally, the unique shape of the tissue in early embryos caused the cells in the center to bear more stress, leading to elongation and a correlation between larger cell sizes and increased tensions. As the dorsal closure progressed, we observed a homogenization in the distribution of tensions, with a noticeable increase along the anteroposterior axis. Through the analysis of genotypes with altered myosin levels, we discovered that cells with less myosin deform more in response to external tensions, indicating that myosin concentrates in the membranes to counteract this stress.

However, although our methods can help measure this type of information, they are far from creating an exact map of tensions and pressures across the tissue. This is because biological tissues are far from simple mechanical constructs under an assumption. Unlike mere ropes, cells within tissues exhibit a

complex dynamic that depends on both mechanical and biochemical factors. This complexity adds a layer of intricacy, especially when it comes to the non-uniform curvature, irregularities, and anomalies observed in the amnioserosa.

Furthermore, we have demonstrated that the quality of segmentation significantly influences the inference results, contributing to the variability observed in our tissue study. This segmentation challenge, coupled with the inherent complexities of biological tissues, underscores the need for a cautious interpretation of our findings.

To validate our results further, experimental validation methods such as laser ablation or the use of stress-responsive proteins would be essential. These methods would provide a more concrete basis for our inferences, bridging the gap between theoretical modeling and real-world biological phenomena.

In conclusion, our research has provided valuable insights into the biomechanical properties of the amnioserosa during dorsal closure, shedding light on specific cellular behaviors and mechanical interactions. These findings pave the way for a more nuanced understanding of tissue mechanics. Nevertheless, our work also highlights the need for more refined models that can account for the multifaceted nature of biological tissues, including both mechanical and biochemical aspects. To truly map tensions within a biological tissue, new models that transcend current assumptions and capture the inherent complexities are essential. Such future developments would facilitate more rigorous, precise analyses, fostering further discoveries in the exciting field of cellular biomechanics.

## References

- Aigouy, B., Umetsu, D., Eaton, S., 2016. Segmentation and Quantitative Analysis of Epithelial Tissues. volume 1478. pp. 227–239. doi:10.1007/978-1-4939-6371-3\_13.
- Blanchard, G.B., Murugesu, S., Adams, R.J., Martinez-Arias, A., Gorfinkiel, N., 2010. Cytoskeletal dynamics and supracellular organisation of cell shape fluctuations during dorsal closure. *Development* 137, 2743–2752.
- Brodland GW, Veldhuis JH, K.S.P.M.M.D.H.M., 2014. Cellfit: A cellular force-inference toolkit using curvilinear cell boundaries .
- Cantat, I., Cohen-Addad, S., Elias, F., Graner, F., Höhler, R., Pitois, O., Rouyer, F., Saint-Jalmes, A., 2013. Foams: structure and dynamics. OUP Oxford.
- Chan, C.J., Heisenberg, C.P., Hiiiragi, T., 2017. Coordination of morphogenesis and cell-fate specification in development. *Current Biology* 27, R1024–R1035.
- Chiou, K.K., Hufnagel, L., Shraiman, B.I., 2012. Mechanical stress inference for two dimensional cell arrays. *PLoS computational biology* 8, e1002512.
- Collinet, C., Lecuit, T., 2021. Programmed and self-organized flow of information during morphogenesis. URL: <https://www.nature.com/articles/s41580-020-00318-6>.
- Ducuing, A., Vincent, S., 2016. The actin cable is dispensable in directing dorsal closure dynamics but neutralizes mechanical stress to prevent scarring in the drosophila embryo. *Nature cell biology* 18, 1149–1160.
- Duque, J., Gorfinkiel, N., 2016. Integration of actomyosin contractility with cell-cell adhesion during dorsal closure. *Development* 143, 4676–4686.
- Fagotto, F., 2014. The cellular basis of tissue separation. *Development* 141, 3303–3318. doi:10.1242/dev.090332.
- Franke, J.D., Montague, R.A., Kiehart, D.P., 2005. Nonmuscle myosin ii generates forces that transmit tension and drive contraction in multiple tissues during dorsal closure. *Current biology* 15, 2208–2221.
- Gjorevski, N., Nelson, C.M., 2010. The mechanics of development: Models and methods for tissue morphogenesis. *Birth Defects Research Part C: Embryo Today: Reviews* 90, 193–202.
- Gorfinkiel, N., Blanchard, G., Adams, R., Arias, A., 2009. Mechanical control of global cell behaviour during dorsal closure in drosophila. *Development* (Cambridge, England) 136, 1889–98. doi:10.1242/dev.030866.
- Gorfinkiel, N., Fischer, S., Blanchard, G., 2011. Integrative approaches to morphogenesis: Lessons from dorsal closure. *Genesis* (New York, N.Y.) : 2000 49, 522–33. doi:10.1002/dvg.20704.
- Graner, F., Riveline, D., 2017. ‘The Forms of Tissues, or Cell-aggregates’: D’Arcy Thompson’s influence and its limits. *Development* 144, 4226–4237. doi:10.1242/dev.151233.
- Guirao, B., Rigaud, S.U., Bosveld, F., Bailles, A., Lopez-Gay, J., Ishihara, S., Sugimura, K., Graner, F., Bellaïche, Y., 2015. Unified quantitative characterization of epithelial tissue development. *Elife* 4, e08519.
- Hannezo, E., Heisenberg, C.P., 2019. Mechanochemical feedback loops in development and disease. *Cell* 178, 12–25.
- Hayes, P., Solon, J., 2017. Drosophila dorsal closure: An orchestra of forces to zip shut the embryo. *Mechanisms of Development* 144, 2–10. URL: <https://www.sciencedirect.com/science/article/pii/S0925477316300983>, doi:<https://doi.org/10.1016/j.mod.2016.12.005>. roles of physical forces in development.
- Heer, N.C., Martin, A.C., 2017. Tension, contraction and tissue morphogenesis. *Development* 144, 4249–4260.
- Hunter, G.L., Crawford, J.M., Jenkins, J.Z., Kiehart, D.P., 2014. Ion channels contribute to the regulation of cell sheet forces during drosophila dorsal closure. *Development* 141, 325–334.
- Hutson, M.S., Tokutake, Y., Chang, M.S., Bloor, J.W., Venakides, S., Kiehart, D.P., Edwards, G.S., 2003. Forces for morphogenesis investigated with laser microsurgery and quantitative modeling. *Science* 300, 145–149.
- Ishihara, S., Sugimura, K., 2012. Bayesian inference of force dynamics during morphogenesis. *Journal of theoretical biology* 313, 201–211.
- Jacinto, A., Wood, W., Woolner, S., Hiley, C., Turner, L., Wilson, C., Martinez-Arias, A., Martin, P., 2002. Dynamic analysis of actin cable function during drosophila dorsal closure. *Current Biology* 12, 1245–1250.
- Jurado, J., de Navascués, J., Gorfinkiel, N., 2016.  $\alpha$ -catenin stabilises cadherin-catenin complexes and modulates actomyosin dynamics to allow pulsatile apical contraction. *Journal of cell science* 129, 4496–4508.
- Kiehart, D.P., Crawford, J.M., Aristotelous, A., Venakides, S., Edwards, G.S., 2017. Cell sheet morphogenesis: dorsal closure in drosophila melanogaster as a model system. *Annual review of cell and developmental biology* 33, 169–202.
- Kiehart, D.P., Galbraith, C.G., Edwards, K.A., Rickoll, W.L., Montague, R.A., 2000. Multiple forces contribute to cell sheet morphogenesis for dorsal closure in drosophila. *The Journal of cell biology* 149, 471–490.
- Krens, S.G., Veldhuis, J.H., Barone, V., Čapek, D., Maître, J.L., Brodland, G.W., Heisenberg, C.P., 2017. Interstitial fluid osmolarity modulates the action of differential tissue surface tension in progenitor cell segregation during gastrulation. *Development* 144, 1798–1806.
- Lv, Z., Zhang, N., Zhang, X., Großhans, J., Kong, D., 2022. The lateral epidermis actively counteracts pulling by the amnioserosa during dorsal closure. *Frontiers in Cell and Developmental Biology* 10, 865397.
- Mammoto, A., Mammoto, T., Ingber, D.E., 2012. Mechanosensitive mechanisms in transcriptional regulation. *Journal of cell science* 125, 3061–3073.
- Miller, C.J., Davidson, L.A., 2013. The interplay between cell signalling and mechanics in developmental processes. *Nature Reviews Genetics* 14, 733–744.
- Mulyil, S., Narasimha, M., 2014. Mitochondrial ros regulates cytoskeletal and mitochondrial remodeling to tune cell and tissue dynamics in a model for wound healing. *Developmental cell* 28, 239–252.
- Noll, N., Streichan, S.J., Shraiman, B.I., 2020. Variational method for image-based inference of internal stress in epithelial tissues. *Physical Review X* 10, 011072.
- Pasakarnis, L., Frei, E., Caussinus, E., Affolter, M., Brunner, D., 2016. Amnioserosa cell constriction but not epidermal actin cable tension autonomously drives dorsal closure. *Nature cell biology* 18, 1161–1172.
- Peralta, X., Toyama, Y., Hutson, M., Montague, R., Venakides, S., Kiehart, D., Edwards, G., 2007. Upregulation of forces and morphogenetic asymmetries in dorsal closure during drosophila development. *Biophysical journal* 92, 2583–2596.
- Roca-Cusachs, P., Conte, V., Trepat, X., 2017. Quantifying forces in cell biology. *Nature cell biology* 19, 742–751.
- Rodriguez-Diaz, A., Toyama, Y., Abravanel, D.L., Wiemann, J.M., Wells, A.R., Tulu, U.S., Edwards, G.S., Kiehart, D.P., 2008. Actomyosin purse strings:

- renewable resources that make morphogenesis robust and resilient. *HFSP journal* 2, 220–237.
- Roffay, C., Chan, C.J., Guirao, B., Hiiragi, T., Graner, F., 2021. Inferring cell junction tension and pressure from cell geometry. *Development* 148, dev192773. doi:10.1242/dev.192773.
- Solon, J., Kaya-Copur, A., Colombelli, J., Brunner, D., 2009. Pulsed forces timed by a ratchet-like mechanism drive directed tissue movement during dorsal closure. *Cell* 137, 1331–1342.
- Stein, M.B., Gordon, R., 1982. Epithelia as bubble rafts: a new method for analysis of cell shape and intercellular adhesion in embryonic and other epithelia. *Journal of Theoretical Biology* 97, 625–639.
- Sumi, A., Hayes, P., D’Angelo, A., Colombelli, J., Salbreux, G., Dierkes, K., Solon, J., 2018. Adherens junction length during tissue contraction is controlled by the mechanosensitive activity of actomyosin and junctional recycling. *Developmental cell* 47, 453–463.
- Taylor, J.E., 1976. The structure of singularities in soap-bubble-like and soap-film-like minimal surfaces. *Annals of Mathematics* 103, 489–539.
- Thomson, J.A., 1917. On growth and form.
- Toyama, Y., Peralta, X.G., Wells, A.R., Kiehart, D.P., Edwards, G.S., 2008. Apoptotic force and tissue dynamics during drosophila embryogenesis. *Science* 321, 1683–1686.
- Vasan, R., Maleckar, M.M., Williams, C.D., Rangamani, P., 2019. Dlite uses cell-cell interface movement to better infer cell-cell tensions. *Biophysical Journal* 117, 1714–1727. URL: <https://www.sciencedirect.com/science/article/pii/S0006349519308215>, doi:<https://doi.org/10.1016/j.bpj.2019.09.034>.